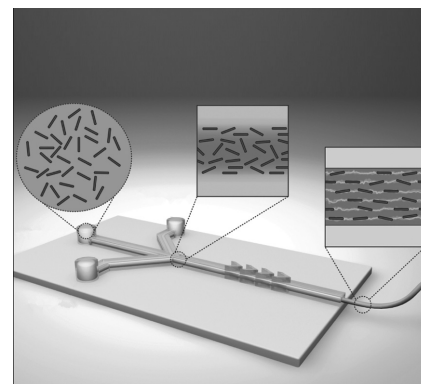


Fluid-Induced Alignment of Carbon Nanofibers in Polymer Fibers

Mingchang Lu, Farrokh Sharifi, Nicole N. Hashemi, Reza Montazami*

Carbon nanofiber/polycaprolactone (CNF/PCL) composite fibers are fabricated using a microfluidic approach. The fibers are made with different content levels of CNFs and flow rate ratios between the core and sheath fluids. The electrical conductivity and tensile properties of these fibers are then investigated. It is found that at a CNF concentration of 3 wt%, the electrical conductivity of the composite fiber significantly increases to 1.11 S m^{-1} . The yield strength, Young's modulus, and ultimate strength of the 3 wt% CNF increase relative to the pure PCL by factors of 1.72, 2.88, and 1.23, respectively. Additionally, the results show that a microfluidic approach can be considered as an effective method to align CNFs along the fibers in the longitudinal direction.



1. Introduction

In recent years, electrically conductive polymer fibers have been extensively investigated due to their promising applications in a wide range of areas, such as static charge dissipation and dust-free clothing,^[1] sensors,^[2–6] actuators,^[7] fiber-based wearable electronics,^[8] energy storage,^[9] drug release,^[10] tissue engineering,^[11] and electromagnetic interference shielding.^[12]

Currently, several approaches have been used to fabricate electrically conductive polymeric fibers. One of the most investigated methods is to directly spin intrinsically conductive polymer (ICP) into fibers via common spinning techniques.^[13] However, the spinning of ICPs is generally very difficult due to their inherent infusibility and insolubility in common solvents.^[14] To make a less difficult ICP spinning solution, some toxic or corrosive solvents have

been used.^[15,16] In addition, the relatively low toughness of ICP fibers limits their application. Another effective way to create a less difficult ICP spinning solution is to coat commercially available fibers with conductive yarns.^[17] ICPs, carbon nanotubes/polymer composites, and other conductive materials have been reported to have been successfully coated onto nonconductive polymer fibers.^[18–24] The coated polymer fibers showed a significantly increase of the conductivity. However, the long-term reliability of the conductive coatings is a concern due to scratching and wearing. In order to avoid the spinning difficulty of ICPs and the unreliability of conductive coating, significant levels of effort has been devoted into the fabrication of conductive filler/polymer composite fibers.

A variety of conductive fillers, such as metal filament,^[25] carbon black,^[26] intrinsically conductive polymer,^[27,28] graphite,^[19] carbon nanotubes,^[29,30] carbon nanofiber,^[31,32] and graphene^[33] have been incorporated into the polymer matrix to fabricate conductive composite materials. In order to significantly increase the conductivity of the resulting polymer matrix, the concentration of the conductive fillers should be above the percolation threshold at which the conductive network is formed by conductive fillers. The optimal conductive fillers should have a high electrical conductivity along with a fairly large aspect ratio which favors the formation of a conductive network and decreases the percolation threshold.^[34,35]

M. Lu, Dr. F. Sharifi, Prof. N. N. Hashemi, Prof. R. Montazami
Department of Mechanical Engineering
Iowa State University
Ames, IA 50011, USA
E-mail: reza@iastate.edu
Prof. N. N. Hashemi, Prof. R. Montazami
Center of Advanced Host Defense Immunobiotics
and Translational Medicine
Iowa State University
Ames, IA 50011, USA

Conventional fiber fabrication techniques, including electrospinning,^[11,36] wet-spinning,^[2,23,37] and melt-spinning^[19,38–40] have been widely reported to assist in making conductive composite fibers. Microfluidics, on the other hand, has shown promising potentials to be used in a wide scope of applications ranging from energy to biomedical industries.^[41–48] Regarding fiber fabrication, the newly emerging microfluidic method has attracted a significant amount of attention by cause of its relatively cheap tooling costs, low consumption of materials, and ability to control the cross-sectional shape of the resulting fibers.^[49] Due to the flexibility of the microfluidic technique, some studies have successfully incorporated cells,^[50] liquid crystals,^[51] and gold nanoparticles^[52] into polymer fibers through the microfluidic method. However, to the best of our knowledge, there has been no report for fabricating electrically conductive composite fibers using a microfluidic platform. In this paper, carbon nanofiber (CNF) and polycaprolactone (PCL), which is a biocompatible and biodegradable polymer, were selected as the electrically conductive filler and the polymer matrix, respectively. Electrically conductive CNF/PCL composite fibers were fabricated using a microfluidic approach for the first time. The electrical conductivity and tensile properties of fibers were studied based on varying CNF content and flow rate ratio.

2. Experimental Section

2.1. Materials

Sylgard 184 Elastomer Base and Curing Agent were obtained from Dow Corning Corporation (Midland, MI). PCL ($M_n = 80\,000$), CNF ($D \times L = 100\text{ nm} \times 20\text{--}200\text{ }\mu\text{m}$), and polyethylene glycol (PEG) ($M_n = 20\,000$) were purchased from Sigma-Aldrich (St. Louis, MO). 2,2,2-trifluoroethanol (TFE) was obtained from Oakwood Chemical (West Columbia, SC).

2.2. Preparation of Microchannel

A microchannel with four chevron grooves on the top and bottom was used for the study. The design of the microchannel is detailed in the Supporting Information. The microchannel was made by bonding two halves of Polydimethylsiloxane (PDMS) using plasma-cleaning. Sylgard 184 Elastomer Base and Curing Agent were mixed with a w/w ratio of 10:1, and then poured over two Poly(methyl methacrylate) (PMMA) molds made by a Computer Numerical Control (CNC) micromilling machine (Mini-Mill-GX, Minitech Machinery Corp.). After curing at 85 °C for 25 min, two half layers of the microchannel were peeled off from the PMMA master molds. The top half layer of the microchannel was bonded with a PDMS substrate via plasma treatment. After waiting for 24 h, three holes were punched as inlets. Then the microchannel was assembled by bonding the top half layer with another half layer via plasma treatment.

2.3. Preparation of Core and Sheath Solutions

Core Fluid: In order to achieve good dispersion of CNFs in PCL solution, CNFs were first dispersed into the PCL solution of low concentration, which was mixed with the PCL solution of high concentration. CNFs were dispersed into a PCL solution of low concentration at 1.25% (0.05 g PCL dissolved in 4 mL TFE). The concentration of the CNFs is with respect to the weight of PCL (i.e., 3 wt% of CNF means that weight ratio of CNFs and PCL is 3:100). After transferring the CNFs suspension, 2 mL of TFE was used to rinse the container in order to capture the residual material. The CNF suspension was magnetically stirred for 30 min then ultrasonicated for another 30 min at room temperature. After preparing the CNFs suspension, it was poured into a PCL/TFE solution of high concentration at 36.25% (1.45 g PCL dissolved in 4 mL TFE) which was thoroughly mixed at 65 °C for 4 h then further mixed at room temperature throughout the rest of the night with constant magnetic stirring. Finally, the suspension was ultrasonicated at 65 °C for 90 min. The CNF suspension was cooled to room temperature during magnetic stirring. Before the fiber fabrication process, the solution was rested for at least 15 min.

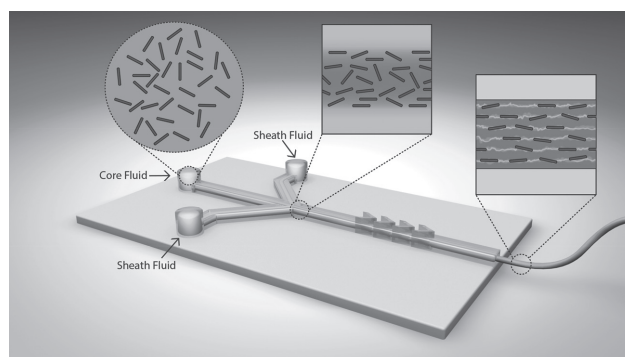
Sheath Fluid: 15% g mL⁻¹ PEG was dissolved into the mixture of DI water and ethanol with a volume ratio of 1:1.

Bath: The mixture of DI water and ethanol at a volume ratio of 1:1 was used as bath for collecting fibers.

The core fluid and sheath fluid were loaded into 3 and 60 mL plastic syringes (BD Biosciences) and pumped into the microchannel using a double syringe pump (Cole-Parmer, Veron Hillss, IL). The core and sheath flow rate ratios were set as 50:10, 40:10, 30:10, and 20 $\mu\text{L min}^{-1}$.

2.4. Microfluidic Fiber Fabrication

The laminar flow regime was used in this experiment. Therefore, the diffusion occurred only at the fluid/fluid interface. Figure 1 shows a schematic of the microfluidic fiber fabrication. As the core and sheath fluids entered the microchannel, the sheath flow exerted lateral hydrodynamic shear force on the core flow at the junction of the three inlets.^[49] As shown in Figure 1, the microchannel has four chevron grooves. Due to the hydrodynamic resistance being inversely dependent on the flow rate and the sheath flow rate having higher values compared to the core flow rate, the sheath fluid filled the chevron grooves at the top and bottom of the microchannel. As a result, the sheath fluid exerted



■ Figure 1. Schematic illustration of microfluidic fiber fabrication.

vertical force on the core fluid as well as lateral force, which resulted in wrapping around the core fluid, and focusing it at the center of the channel.^[45] In this process, the shear force played a significant role in changing the shape of the resulting fiber as well as aligning the CNFs and polymer chain along the flow direction. The phase inversion solidification strategy was used in this process, which means that the molecules of the TFE were replaced by the molecules of the sheath fluid (water and ethanol) at the core/sheath interface. Because PCL was not soluble in the sheath fluid, it was solidified as a fiber at the outlet of the channel.

2.5. Characterization

The morphology and cross-sectional properties of the prepared fibers were investigated using scanning electron microscopy (NeoScopo, JCM-6000 Benchtop SEM) and the Dino Lite microscope. Five specimens were measured to calculate the fiber dimensions. The conductivity of the fibers was measured based on a bundle of 1000 fibers with a length of 10 mm as shown in Figure S5a (Supporting Information) and single fiber with a length of 500 μm as shown in Figure S5b,c (Supporting Information). The current was measured while applied voltage increased from -10 to $+10$ V using the potentiostat (Princeton Applied Research, Versa STAT 4). Linear regression was used for the voltage and current to calculate the resistance. The conductivity of the fibers (ρ) was calculated based on the measured resistance (R), length (L), and cross-sectional area (A) with the following equation

$$\rho = RA/L \quad (1)$$

A single fiber with a gauge length of 10 mm was used for the measurement of the tensile properties based on ASTM Standard D3822/D3822M-14 using Instron Universal Testing Machine (Model 5560, Instron Engineering Corp., Canton, MA). For all of the tests, a 10 N loading cell was used. The extension rate was set to 24 mm min^{-1} , and 20 specimens were tested for each sample.

3. Results and Discussion

3.1. Morphology

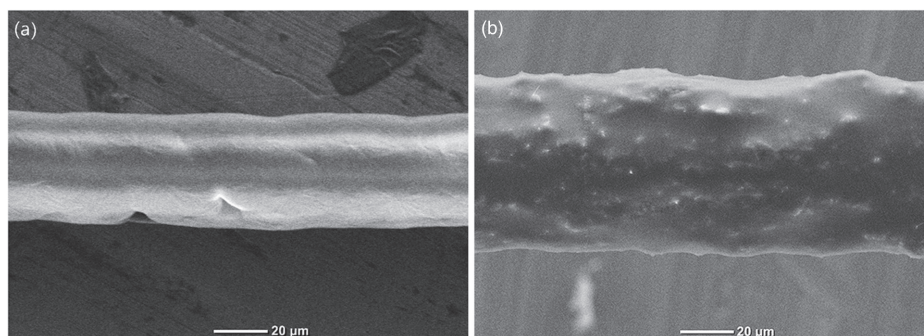
The SEM images of pure PCL fibers and 5% CNF/PCL composite fibers obtained with the sheath-to-core flow rate

ratio of 50:10 $\mu\text{L min}^{-1}$ are shown in Figure 2. The incorporation of CNF into PCL changes the morphology of the fibers significantly. While pure PCL fibers exhibit smooth surfaces and uniform diameter along the longitudinal direction, the CNF/PCL composite fibers have a significantly higher surface roughness. The increase in surface roughness was expected because the CNFs decrease the uniformity of the pure PCL solution, which results in the fabrication of fibers with high surface roughness. Additionally, the uniformity of the fiber diameter decreased which might due to the nonuniform dispersion of the CNFs in the core flow solution.

Furthermore, the addition of CNF increases the viscosity of the core fluid. A higher viscosity of the core flow results in a weakened hydrodynamic focusing from the sheath flow. Thus, the width of the core fluid in the channel increases, hence the resulting CNF/PCL composite fibers will have larger dimensions.

As shown in Figure 3, a higher flow rate ratio tended to give a more circular cross-sectional shape, and the addition of CNFs increased the cross-sectional area of the fibers. At lower flow rate ratio, the hydrodynamic focusing applied on core fluid by the sheath fluid was weaker. As a result, the fiber could grow more in lateral direction. For the vertical direction, the hydrodynamic focusing was determined by both flow rate ratio and the chevron shaped grooves on the top and bottom of the microchannel, so the increase of fiber dimension was less significant.

Detailed dimensions of fibers with different concentration of CNFs and different flow rate ratios are shown in Figure 4a,b. For pure PCL fibers, the short axis increased from 35.32 to 39.1 μm and long axis increased from 46.22 to 52.01 μm when the flow rate ratio decreased from 50:10 to 20:10. Moreover, the aspect ratio slightly increased from 1.31 to 1.33. For 2.5 wt% CNF/PCL fibers, the dimension changes more radically with changes in the flow rate ratio compared with pure PCL fibers. As the flow rate ratio decreased from 50:10 to 20:10, the short axis, long axis and aspect ratio increased from 35.36 to 43.50 μm , 61.25 to 87.44 μm , and 1.73 to 2.01, respectively. The change



■ Figure 2. SEM Images of a) PCL and b) 5 wt% CNF/PCL composite fibers.

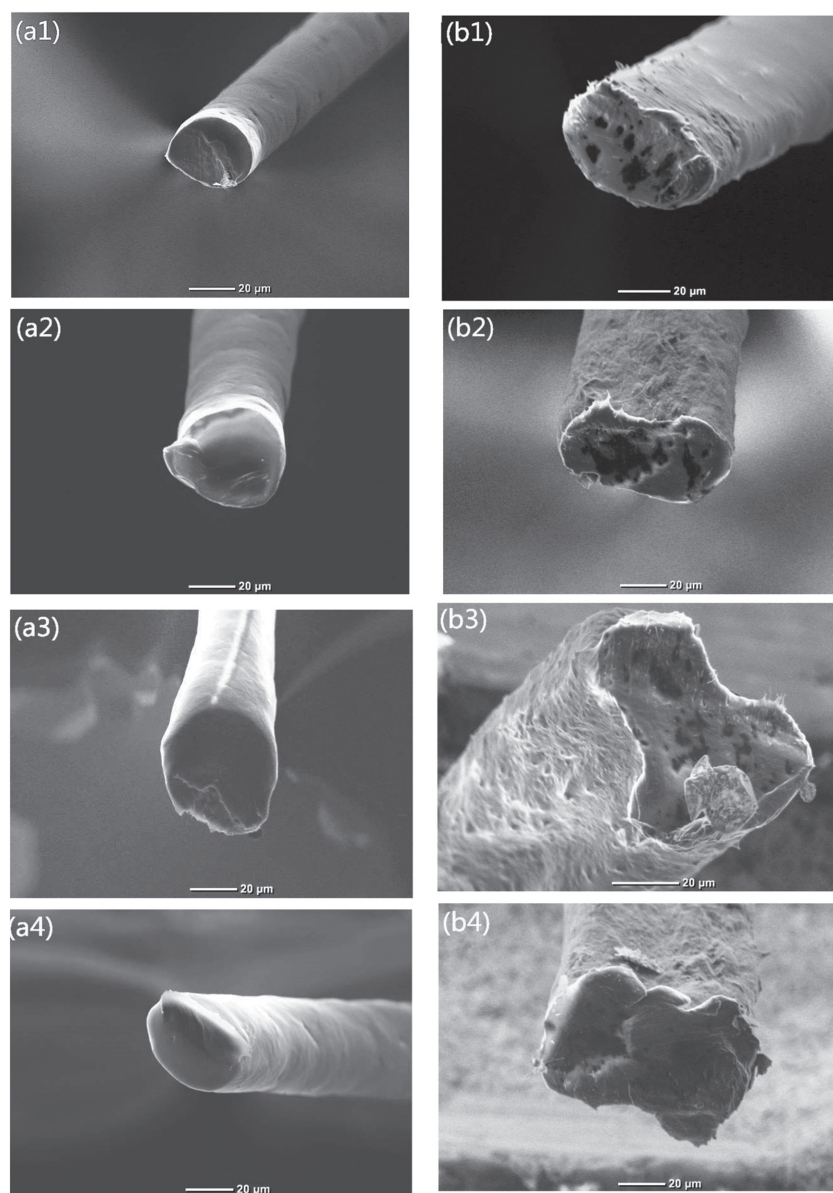


Figure 3. Cross-sectional SEM images of a1–a4) PCL fibers (sheath-to-core flow rate ratio: a₁–a₄: 50:10, 40:10, 30:10, 20:10, respectively). b) 2.5 wt% CNF/PCL fibers (b₁–b₄: 50:10, 40:10, 30:10, 20:10, respectively).

in morphology and size of the fibers is likely due to the weakened hydrodynamic focusing caused by increased core fluid and a smaller flow rate ratio. Additionally, the short axis, long axis, and aspect ratio of fibers made with a flow rate ratio of 50:10 increased from 35.32, 44.2, 46.22 to 62.13 μm and 1.31 to 1.41, respectively, as the concentration of CNF increased from 0 to 5 wt%. The change of the dimensions might also result from weakened hydrodynamic focusing. The incorporation of CNFs could lead to increasing of the core fluid viscosity, which would result in weakened hydrodynamic focusing.^[45] Also, the

rigid CNFs could also restrict the hydrodynamic focusing.

Figure 5a,b shows the cross-sectional SEM image of the pure PCL fiber and CNF/PCL composite fibers with higher magnification, and the SEM images of CNFs incorporated into PCL microfibers, respectively. We poured several drops of TFE, the solvent of PCL, on the CNF/PCL composite fibers in order to wash the PCL portion and be able to observe the CNFs clearly. Compared to the smooth section of the PCL fiber, the cross-section of the CNF/PCL composite fiber exhibits high surface roughness as a result of CNFs protruding out along the longitudinal direction of the fiber. The protruded CNFs provide evidence for their alignment along the longitudinal direction. The alignment of the CNFs could be explained as follows.^[51] As the velocity of the flow in the channel distributes parabolically, the flow undergoes a shear force and its magnitude is a function of the distance from the walls of the microchannel. As the aspect ratio of the CNFs is significantly larger than 1, the CNFs could have a tendency of alignment due to the shear force. Before the conjunction of the core and sheath flows, the core fluid experiences a shear in the rectangular channel. Based on the distribution of the fluid velocity, a smaller distance from the microchannel walls results in larger shear rates due to the high velocity gradient. Although the shear rate is smaller because of the smaller core flow rate, it takes more time for the core flow to pass the relatively long inlet channel, which makes this part play an important role for the alignment of the CNFs. During hydrodynamic focusing, the core flow would be accelerated to match the speed of the sheath flow. As the core fluid spans the microchannel in the vertical direction at a location before the chevron grooves, the speed of the core flow along the vertical direction still possesses nonuniformity, which could also lead to shear forces. While the core fluid passes the pre-chevron groove region faster, accelerated core flow would result in larger shear rates. In addition, the elongational flows generated by hydrodynamic focusing could contribute to the alignment of the CNFs.

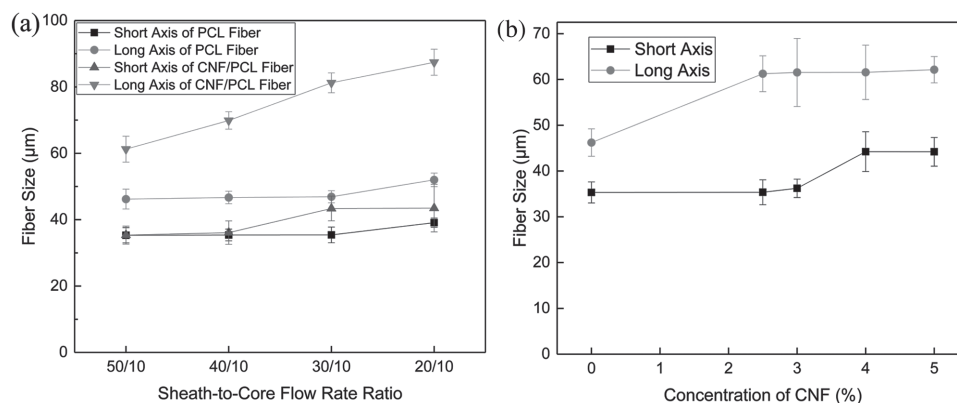


Figure 4. Dimensions of fibers with a) pure PCL and 2.5 wt% CNF/PCL made with different sheath-to-core flow rate ratios. b) Fibers with different concentrations of CNF made with sheath-to-core flow rate ratio of 50:10.

3.2. Electrical Conductivity

Linear regression of current and voltage was performed in R Language to obtain the resistance. Acceptable linearity between current and voltage were found with a coefficient of determination R^2 larger than 0.98. Typical current–voltage fitting lines are shown in Figure S6 (Supporting Information).

CNF/PCL composite fibers exhibited noncontinuous conductivity as the concentration of the CNFs were lower than 3 wt%. This lead to the conductivity of the single-fiber specimens to be tested only with CNF concentrations higher than 3 wt%. Figure 6 shows the change of the electrical conductivity of the CNF/PCL fibers as a function of CNF concentration. The resistance of the composite fibers reached detectable levels as the concentration of CNFs increased to 2.25 wt%. Originally, the conductivity of the composite fibers increased significantly with the increasing of CNFs concentration. As shown in Table 1, the electrical conductivity increased from 5.47×10^{-3} to 1.11 S m^{-1} while the concentration of CNFs increased from 2.25 to 3 wt%. Compared with the conductivity of PCL (lower than 10^{-6} S m^{-1} , beyond the measurable range), there was a significant increase. As the concentration of CNFs reached 3 wt%, the rate of increasing conductivity decreased. Rising the

concentration of the CNFs from 3 to 5 wt%, the conductivity increased slightly from 1.11 to 8.02 S m^{-1} based on the 1000-fiber bundle specimen and from 1.96 to 4.02 S m^{-1} based on the single-fiber specimen. In addition, the conductivity values which were measured based on the 1000-fiber bundle and single-fiber specimen were comparatively close, which provided evidence for the continuity of conductivity.

In order to investigate the continuity of conductivity, ten single-fiber samples of 2.5 wt% CNF/PCL composite fibers from different flow rate ratios were measured using a digital multimeter. As shown in Table 2, a lower flow rate ratio shows more continuous conductivity. Table 3 shows the conductivity of 2.5 wt% CNF/PCL composite fibers measured based on the bundle of 1000 fibers.

The pure PCL fibers were white and semitransparent and the color changed to dark while the transparency decreased as PCL incorporated with CNFs (showed in Figure S7, Supporting Information). For 2.5 wt% CNF/PCL fiber, some discontinuous and partially CNF-filled PCL regions were observed. As the concentration of CNF increased to 3 wt%, no discontinuous region was found. For the 2.5 wt% CNF/PCL fiber, the CNFs were not enough to fully fill the PCL matrix, which led to a noncontinuous distribution and low conductivity. For a lower flow rate

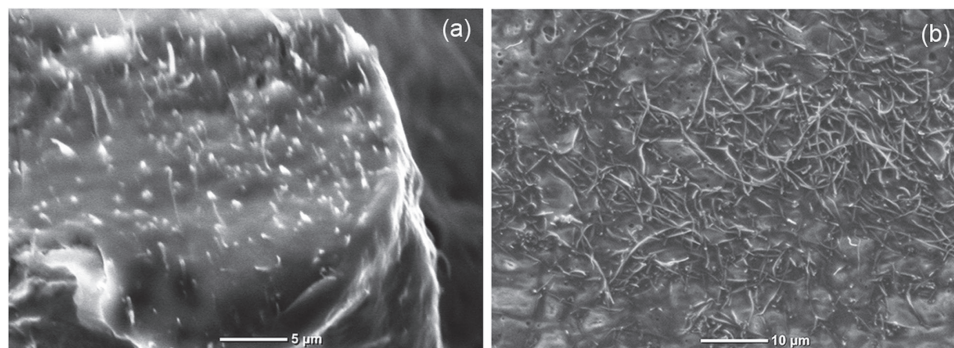


Figure 5. a) Cross-sectional SEM images of 5 wt% CNF/PCL composite fiber made from flow rate ratio of 50:10. b) SEM images of CNFs incorporated into PCL microfluidic-spun fibers.

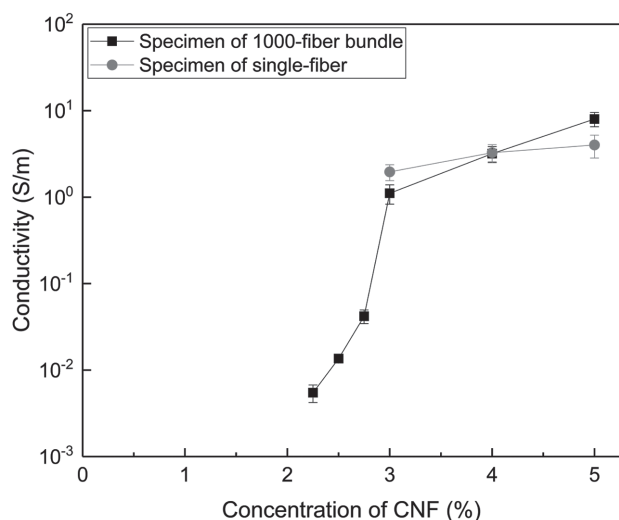


Figure 6. Conductivity of fibers as a function of CNF concentration.

ratio, the core flow would take more space in the micro-channel, which would result in fibers with larger cross-sectional areas. This suggests that the probability of the conductivity discontinuity might be decreased. On the other hand, a higher flow rate ratio produced larger shear forces during the hydrodynamic focusing, which aligns the CNFs along the fiber direction. The alignment of the CNFs is helpful for obtaining higher conductivity. These two competitive factors made the conductivity of 2.5 wt% CNF/PCL 1000-fiber bundle increase from $(1.36 \pm 0.15) \times 10^{-2} \text{ S m}^{-1}$ at the sheath-to-core flow rate of 50/10 to $(1.28 \pm 0.18) \times 10^{-1} \text{ S m}^{-1}$ at the sheath-to-core flow rate of 30/10 and then decreased to $(5.97 \pm 1.42) \times 10^{-2} \text{ S m}^{-1}$ as the sheath-to-core flow rate ratio changed to 20/10 (as shown in Figure 7 and Table 3).

Table 3 also shows the conductivity of 5 wt% CNF/PCL composite fibers measured based on a single fiber. As the CNF concentration of 5 wt% is high enough for producing continuous conductivity, the conductivity of the composite fiber is mainly determined by the alignment of the CNFs. As lower flow rate ratios resulted in smaller shear stress during the hydrodynamic focusing, the alignment of the CNFs was weakened. As a result, the conductivity of the composite fibers decreased from 4.02 to 2.63 S m^{-1} when the flow rate ratio was decreased from 50:10 to 20:10. However, as the concentration of the CNFs already

Table 2. Percentage of resistance-undetectable of 2.5 wt% CNF/PCL fibers.

Sheath-to-core flow Rate ratio	50/10	40/10	30/10	20/10
Percentage of undetectable samples	4/10	4/10	2/10	1/10

exceeded the percolation, the change of the conductivity was very small.

3.3. Tensile Properties

Typical of the strain–stress curves for the PCL and PCL/CNF is shown in Figure S8 (Supporting Information). At the beginning, the tensile strength of the fiber increased with increasing the concentration of CNFs. As the concentration of the CNFs reached 3 wt%, the strength started decreasing by further increasing the CNFs concentration. That might be due to the voids produced by the agglomeration of the CNFs at a high concentration. The tensile strength of 2.5 wt% CNF/PCL composite fibers fabricated with different flow rate ratios was also investigated. It concluded that a higher flow rate ratio tends to result in fibers with a higher strength. As mentioned in the previous section, a larger flow rate ratio would produce a larger shear rate during the hydrodynamic focusing, which would be helpful for aligning the CNFs as well as PCL polymer chain along the fiber direction. This leads to the realization that increased tensile strength can be ascribed to the alignment of the CNFs.

The detailed tensile properties of the PCL and CNF/PCL fibers are provided in Table 4. For the PCL fibers, the tensile strength had a tendency of increasing and then decreasing as the sheath to core flow rate ratio increased. Two competitive factors may play a role for the change of the tensile strength with the flow rate ratio. For higher flow rate ratios, the resulting fibers have smaller cross-sectional areas, which indicate the occurrence probability of voids is smaller. The failure of material starts from the voids and then the propagation of cracks finally leads to the breaking-down of the material. Owing to smaller occurrence probability of voids could be endowed by higher flow rate ratios, fibers fabricated with higher flow rate ratio show higher tensile strength.

Table 1. Conductivity of composite fibers with different CNF concentration (sheath-to-core flow rate ratio = 50/10).

Weight ratio (CNF/PCL)	2.25/100	2.5/100	2.75/100	3/100	4/100	5/100
Conductivity [S m^{-1}] (measured based on 1000-fiber bundle)	$(5.47 \pm 1.25) \times 10^{-3}$	$(1.36 \pm 0.15) \times 10^{-2}$	$(4.20 \pm 0.75) \times 10^{-2}$	1.11 ± 0.28	3.19 ± 0.65	8.02 ± 1.50
Conductivity [S m^{-1}] (measured based on single fiber)	–	–	–	1.96 ± 0.41	3.27 ± 0.77	4.02 ± 1.19

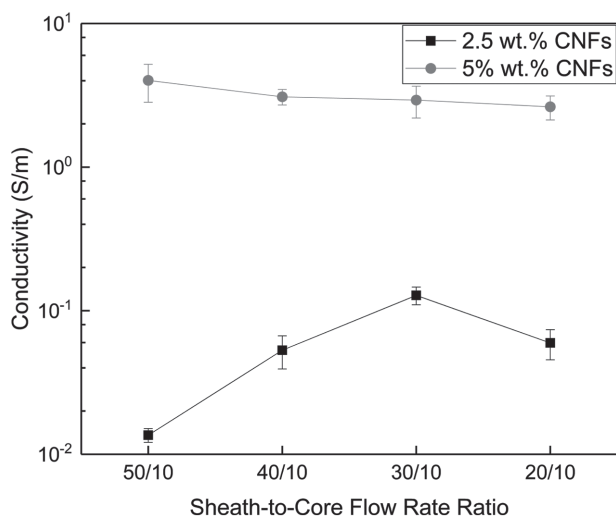
■ Table 3. Conductivity of composite fibers fabricated by using different flow rate ratios.

Flow rate ratio (sheath flow/core flow)	50/10	40/10	30/10	20/10
Conductivity of 2.5 wt% CNF/PCL fiber [$S m^{-1}$] (measured based on 1000-fiber bundle)	$(1.36 \pm 0.15) \times 10^{-2}$	$(5.31 \pm 1.38) \times 10^{-2}$	$(1.28 \pm 0.18) \times 10^{-1}$	$(5.97 \pm 1.42) \times 10^{-2}$
Conductivity [$S m^{-1}$] 5 wt% CNF/PCL fiber [$S m^{-1}$] (measured based on single fibers)	4.02 ± 1.19	3.09 ± 0.38	2.93 ± 0.73	2.63 ± 0.50

■ Table 4. Tensile properties of PCL and CNF/PCL fibers.

Weight ratio (CNF/PCL)	Flow rate ratio (sheath flow/core flow)	Cross-sectional dimensions (short axis/long axis, μm)	Yield strength [MPa]	Young's modulus [MPa]	Failure strength [MPa]	Elongation at break
0/100	50/10	$35.3 \pm 2.3/46.2 \pm 3.0$	8.8 ± 0.5	322.6 ± 23.6	40.1 ± 1.9	7.4 ± 0.2
	40/10	$35.4 \pm 1.8/46.7 \pm 1.9$	9.3 ± 0.4	334.3 ± 14.0	41.6 ± 1.7	7.4 ± 0.1
	30/10	$35.4 \pm 2.3/46.9 \pm 1.8$	8.9 ± 0.4	317.2 ± 17.2	37.0 ± 1.1	6.8 ± 0.2
	20/10	$39.1 \pm 1.4/52.0 \pm 2.0$	7.7 ± 0.5	287.6 ± 16.0	29.8 ± 1.6	6.5 ± 0.2
2.5/100	50/10	$35.4 \pm 2.7/61.3 \pm 3.9$	14.1 ± 0.3	820.2 ± 35.8	48.2 ± 1.4	7.6 ± 0.2
	40/10	$36.1 \pm 3.5/69.9 \pm 2.6$	11.8 ± 0.5	665.9 ± 35.9	41.7 ± 1.8	7.5 ± 0.2
	30/10	$43.4 \pm 3.7/81.2 \pm 3.0$	10.9 ± 0.3	594.8 ± 22.5	37.0 ± 1.3	7.2 ± 0.2
	20/10	$43.5 \pm 7.2/87.4 \pm 3.9$	10.0 ± 0.2	537.6 ± 25.8	33.0 ± 1.6	7.3 ± 0.2
3/100	50/10	$36.2 \pm 2.0/61.5 \pm 7.4$	15.2 ± 0.9	929.6 ± 51.3	49.2 ± 2.4	7.6 ± 0.3
4/100	50/10	$44.2 \pm 4.3/61.6 \pm 5.9$	8.6 ± 0.3	562.4 ± 13.4	34.4 ± 1.1	6.8 ± 0.1
5/100	50/10	$44.2 \pm 3.1/62.1 \pm 2.9$	8.6 ± 0.5	556.5 ± 25.6	24.1 ± 1.4	5.0 ± 0.5

However, decreasing the flow rate ratio could increase the aspect ratio of the fibers, which was demonstrated to endow fibers with higher strength.^[45] As shown in Section 3.1, because the change of aspect ratio is very small, the decreasing of the cross-sectional area might play a more important role. For the samples with the



■ Figure 7. Conductivity of fibers made by using different sheath-to-core flow rate ratios and CNF concentrations of 2.5 and 5 wt%.

CNF concentration of 2.5 wt%, the yield strength, Young's modulus and ultimate strength of the fibers fabricated with the sheath-to-core flow rate ratio of 50:10 were 1.41, 1.53, and 1.46 times of fibers fabricated with the flow rate ratio of 20:10, respectively. The addition of CNFs with a concentration of 3 wt% resulted in the maximum tensile strength. The yield strength, Young's modulus, and ultimate strength of 3 wt% CNF/PCL composite fiber were 15.21, 929.57, and 49.21 MPa, which were, respectively, 1.72, 2.88, and 1.23 times of the pure PCL fiber.

4. Conclusions

In this paper, electrically conductive CNF/PCL composite fibers were fabricated using a microfluidic approach for the first time. Morphology, electrically conductivity, and tensile strength of the resulting composite fibers were studied as a function of the flow rate ratio and CNF content. Compared to traditional fiber spinning techniques, it was demonstrated that the cross-sectional size and aspect ratio of the fibers can be adjusted using the microfluidic platform. The addition of CNFs in to PCL matrix significantly increased the conductivity of the fibers. At CNFs content level of 3 wt%, the conductivity of composite

fiber reached 1.11 S m^{-1} . In addition, it was found that CNFs could be aligned along the fiber longitudinal direction by the shear force during microfluidic fabrication process. The alignment of CNFs played a positive role on increasing the fiber conductivity. At the same time, the tensile properties of the fibers were also improved due to the incorporation of CNFs. We showed that the yield strength, Young's modulus, and tensile strength increased to 1.72, 2.88, and 1.23 times of pure PCL fiber with the addition of 3 wt% CNFs. We noticed that by increasing the CNFs content to the values higher than 3 wt%, the conductivity increased slightly, while the tensile strength dropped sharply, which might be due to the agglomeration of CNFs. In conclusion, microfluidics can be considered as a functional approach to fabricate electrically conductive CNF/PCL composite fibers with controllable cross-sectional size and shape, and align CNFs along the fiber longitudinal direction. These fibers can play important roles in a variety of areas ranging from energy to biomedical applications.

Supporting Information

Supporting Information is available from the Wiley Online Library or from the author.

Acknowledgements: This work was supported by the Office of Naval Research (Grant No. N000141612246) and the Iowa State University Presidential Initiative for Interdisciplinary Research. The authors would also like to thank Ashley Christopherson for illustrating the microfluidic fiber fabrication approach.

Received: December 12, 2016; Revised: February 27, 2017;
Published online: April 11, 2017; DOI: 10.1002/mame.201600544

Keywords: electrical conductivity; polymer fibers; tensile properties

- [1] H. Deng, T. Skipa, E. Bilotti, R. Zhang, D. Lellinger, L. Mezzo, Q. Fu, I. Alig, T. Peijs, *Adv. Funct. Mater.* **2010**, *20*, 1424.
- [2] S. Seyedin, J. M. Razal, P. C. Innis, A. Jeiranikhameneh, S. Beirne, G. G. Wallace, *ACS Appl. Mater. Interfaces* **2015**, *7*, 21150.
- [3] T. K. Bera, Y. Mohamadou, K. Lee, H. Wi, T. I. Oh, E. J. Woo, M. Soleimani, J. K. Seo, *Sensors* **2014**, *14*, 9738.
- [4] C. Cochrane, M. Lewandowski, V. Koncar, *Sensors* **2010**, *10*, 8291.
- [5] C. Li, E. T. Thostenson, T.-W. Chou, *Compos. Sci. Technol.* **2008**, *68*, 1227.
- [6] K. Cherenack, C. Zysset, T. Kinkeldei, N. Münzenrieder, G. Tröster, *Adv. Mater.* **2010**, *22*, 5178.
- [7] B. Qi, W. Lu, B. R. Mattes, *J. Phys. Chem. B* **2004**, *108*, 6222.
- [8] W. Zeng, L. Shu, Q. Li, S. Chen, F. Wang, X. M. Tao, *Adv. Mater.* **2014**, *26*, 5310.
- [9] L. Bao, X. Li, *Adv. Mater.* **2012**, *24*, 3246.
- [10] M. R. Abidian, D. H. Kim, D. C. Martin, *Adv. Mater.* **2006**, *18*, 405.
- [11] L. Ghasemi-Mobarakeh, M. P. Prabhakaran, M. Morshed, M. H. Nasr-Esfahani, H. Baharvand, S. Kiani, S. S. Al-Deyab, S. Ramakrishna, *J. Tissue Eng. Regen. Med.* **2011**, *5*, e17.
- [12] S. Shinagawa, Y. Kumagai, K. Urabe, *J. Porous Mater.* **1999**, *6*, 185.
- [13] Y. Zhang, G. C. Rutledge, *Macromolecules* **2012**, *45*, 4238.
- [14] R. Gangopadhyay, A. De, *Chem. Mater.* **2000**, *12*, 608.
- [15] A. Andreatta, Y. Cao, J. C. Chiang, A. J. Heeger, P. Smith, *Synth. Met.* **1988**, *26*, 383.
- [16] A. Andreatta, S. Tokito, P. Smith, A. Heeger, *Mol. Cryst. Liq. Cryst.* **1990**, *189*, 169.
- [17] M. Stoppa, A. Chiolerio, *Sensors* **2014**, *14*, 11957.
- [18] Y. Ding, M. A. Invernale, G. A. Sotzing, *ACS Appl. Mater. Interfaces* **2010**, *2*, 1588.
- [19] B. Kim, V. Koncar, E. Devaux, C. Dufour, P. Viallier, *Synth. Met.* **2004**, *146*, 167.
- [20] D. Knittel, E. Schollmeyer, *Synth. Met.* **2009**, *159*, 1433.
- [21] T. Bashir, L. Fast, M. Skrifvars, N. K. Persson, *J. Appl. Polym. Sci.* **2012**, *124*, 2954.
- [22] B. S. Shim, W. Chen, C. Doty, C. Xu, N. A. Kotov, *Nano Lett.* **2008**, *8*, 4151.
- [23] P. Xue, K. Park, X. Tao, W. Chen, X. Cheng, *Compos. Struct.* **2007**, *78*, 271.
- [24] C. Robert, J. F. o. Feller, M. Castro, *ACS Appl. Mater. Interfaces* **2012**, *4*, 3508.
- [25] Y. Zhu, Y. Zhao, X. Zhang, L. Wang, X. Wang, J. Zhang, P. Han, J. Qiao, *Mater. Lett.* **2016**, *173*, 26.
- [26] X. Jin, C. Xiao, C. Yu, C. Xie, *Chin. J. Mater. Res.* **2010**, *24*, 311.
- [27] B. Zhang, T. Xue, J. Meng, H. Li, *J. Text. Inst.* **2015**, *106*, 253.
- [28] B. S. Spearman, A. J. Hodge, J. L. Porter, J. G. Hardy, Z. D. Davis, T. Xu, X. Zhang, C. E. Schmidt, M. C. Hamilton, E. A. Lipke, *Acta Biomater.* **2015**, *28*, 109.
- [29] J. Jeong, J. Moon, S. Jeon, J. Park, P. Alegaonkar, J. Yoo, *Thin Solid Films* **2007**, *515*, 5136.
- [30] A.-T. Chien, P. V. Gulgunje, H. G. Chae, A. S. Joshi, J. Moon, B. Feng, G. Peterson, S. Kumar, *Polymer* **2013**, *54*, 6210.
- [31] R. Jain, H. G. Chae, S. Kumar, *Compos. Sci. Technol.* **2013**, *88*, 134.
- [32] M. Sanchez-Garcia, J. Lagaron, S. Hoa, *Compos. Sci. Technol.* **2010**, *70*, 1095.
- [33] S. Sayyar, E. Murray, B. C. Thompson, S. Gambhir, D. L. Officer, G. G. Wallace, *Carbon* **2013**, *52*, 296.
- [34] Y. Yu, S. Song, Z. Bu, X. Gu, G. Song, L. Sun, *J. Mater. Sci.* **2013**, *48*, 5727.
- [35] J. Y. Yi, G. M. Choi, *J. Electroceram.* **1999**, *3*, 361.
- [36] B. Sundaray, V. Subramanian, T. Natarajan, K. Krishnamurthy, *Appl. Phys. Lett.* **2006**, *88*, 143114.
- [37] R. Ma, J. Lee, D. Choi, H. Moon, S. Baik, *Nano Lett.* **2014**, *14*, 1944.
- [38] T. H. Lim, S. H. Lee, S. Y. Yeo, *Text. Res. J.* **2016**, *87*, 593.
- [39] R. Haggemueller, H. Gommans, A. Rinzler, J. E. Fischer, K. Winey, *Chem. Phys. Lett.* **2000**, *330*, 219.
- [40] T. Fornes, J. Baur, Y. Sabba, E. Thomas, *Polymer* **2006**, *47*, 1704.
- [41] D. Sinton, *Lab Chip* **2014**, *14*, 3127.
- [42] S. M. Mitrovski, L. C. C. Elliott, R. G. Nuzzo, *Langmuir* **2004**, *20*, 6974.
- [43] F. Sharifi, S. Ghobadian, F. R. Cavalcanti, N. Hashemi, *Renewable Sustainable Energy Rev.* **2015**, *52*, 1453.

- [44] F. Sharifi, A. C. Sooriyachchi, H. Altural, R. Montazami, M. N. Rylander, N. Hashemi, *ACS Biomater. Sci. Eng.* **2016**, *2*, 1411.
- [45] F. Sharifi, D. Kurteshi, N. Hashemi, *J. Mech. Behav. Biomed. Mater.* **2016**, *61*, 530.
- [46] P. J. Goodrich, F. Sharifi, N. Hashemi, *RSC Adv.* **2015**, *5*, 71203.
- [47] F. Sharifi, Z. Bai, R. Montazami, N. Hashemi, *RSC Adv.* **2016**, *6*, 55343.
- [48] N. Hashemi, J. M. Lackore, F. Sharifi, P. J. Goodrich, M. L. Winchell, N. Hashemi, *Technology* **2016**, *04*, 98.
- [49] Z. Bai, J. M. M. Reyes, R. Montazami, N. Hashemi, *J. Mater. Chem. A* **2014**, *2*, 4878.
- [50] Y. Jun, M. J. Kim, Y. H. Hwang, E. A. Jeon, A. R. Kang, S.-H. Lee, D. Y. Lee, *Biomaterials* **2013**, *34*, 8122.
- [51] A. R. Shields, C. M. Spillmann, J. Naciri, P. B. Howell, A. L. Thangawng, F. S. Ligler, *Soft Matter* **2012**, *8*, 6656.
- [52] D. A. Boyd, J. Naciri, J. Fontana, D. B. Pacardo, A. R. Shields, J. Verbar, C. M. Spillmann, F. S. Ligler, *Macromolecules* **2014**, *47*, 695.